CHAPTER THREE

Insights Into the Electro-oxidation of Hydrazine at Single-Walled Carbon-Nanotube-Modified Edge-Plane Pyrolytic Graphite Electrodes Electrodecorated with Metal and Metal Oxide Films*

* The publication below resulted from part of the research work presented in this chapter and it is not referenced further in this thesis:

1. **Abolanle S. Adekunle**, Kenneth I. Ozoemena, *J. Solid State Electrochem*. 12 (2008)1325-1336.

3.1 Comparative FESEM images and Electron-Dispersive X-rays.

Figure 3.1 compares the SEM images of the bare EPPGE, EPPGE-SWCNT and EPPGE-SWCNT-Ni. The edge-plane sites of the EPPGE are evident in its SEM image (a).

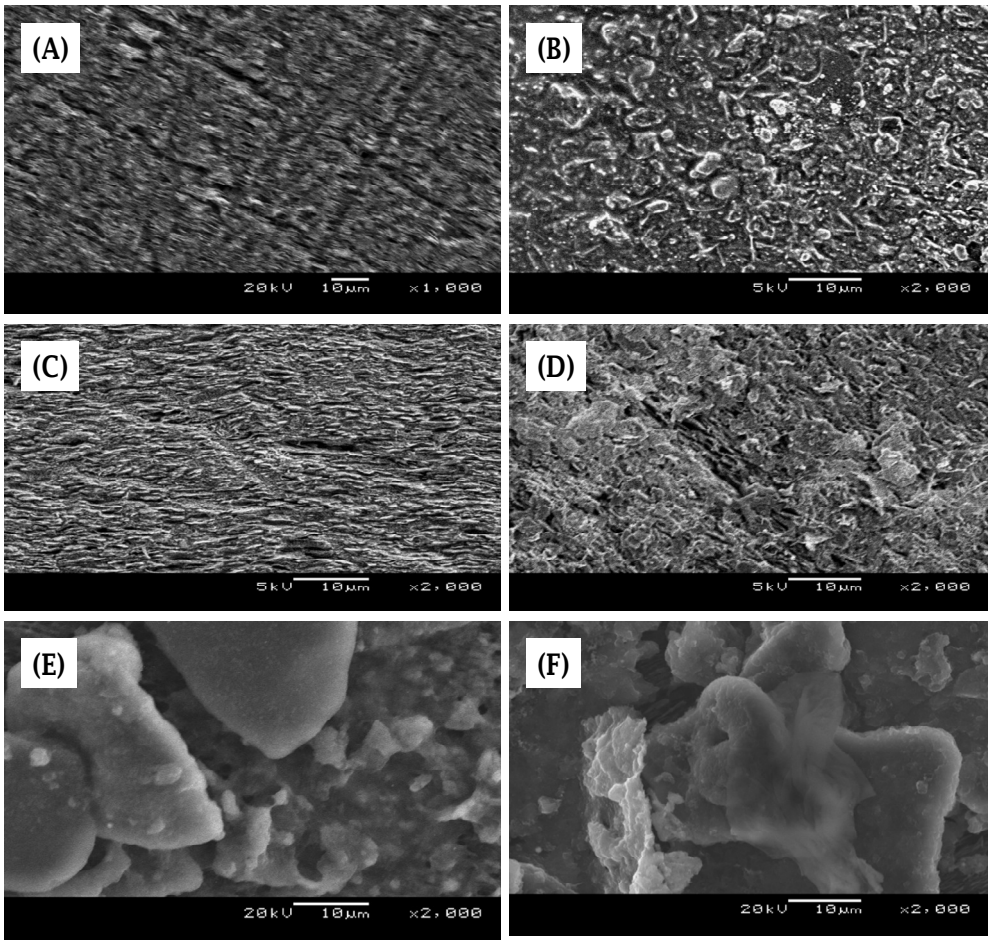

Figure 3.1: Typical FESEM images of the (a) bare EPPGE, (b) EPPGE- SWCNT, (c) EPPGE-SWCNT-Ni, (d) EPPGE-SWCNT-Fe, (e) EPPGE-SWCNT-NiO and (f) EPPGE-SWCNT-FeO.

Upon modification of the EPPGE with the acid-treated and washed SWCNTs, the morphology shows aggregated SWCNTs (b). Upon introduction of the metal particles, an interconnected layer-structured network image of the SWCNT-modified EPPGE (c and d) was observed. However, upon electrochemical treatment in aqueous solution these layer-structured networks become disconnected

transforming into lumps with exposed interiors (e and f), with sizes in the micrometer ranges. As also speculated by other workers [1,2]. It may be reasonable to assume here that these metal particles could either be trapped in the graphite layers and/or located on the outside of the tubes exposed to the solutions, and/or mixed amongst the aggregated bundles of the tubes. To corroborate the SEM results, EDX experiments were run at the various electrodes. The EDX profile (Figure 3.2) gives the analytical details of the elemental composition of the different electrodes. As expected, the unmodified EPPGE (a) predominantly showed carbon. The acid-treated SWCNT (b) confirmed presence of oxo-funtionalities, with sulphur peak which could have arisen from the sulphuric acid solution used in the fuctionalization and washing of the SWCNTs.

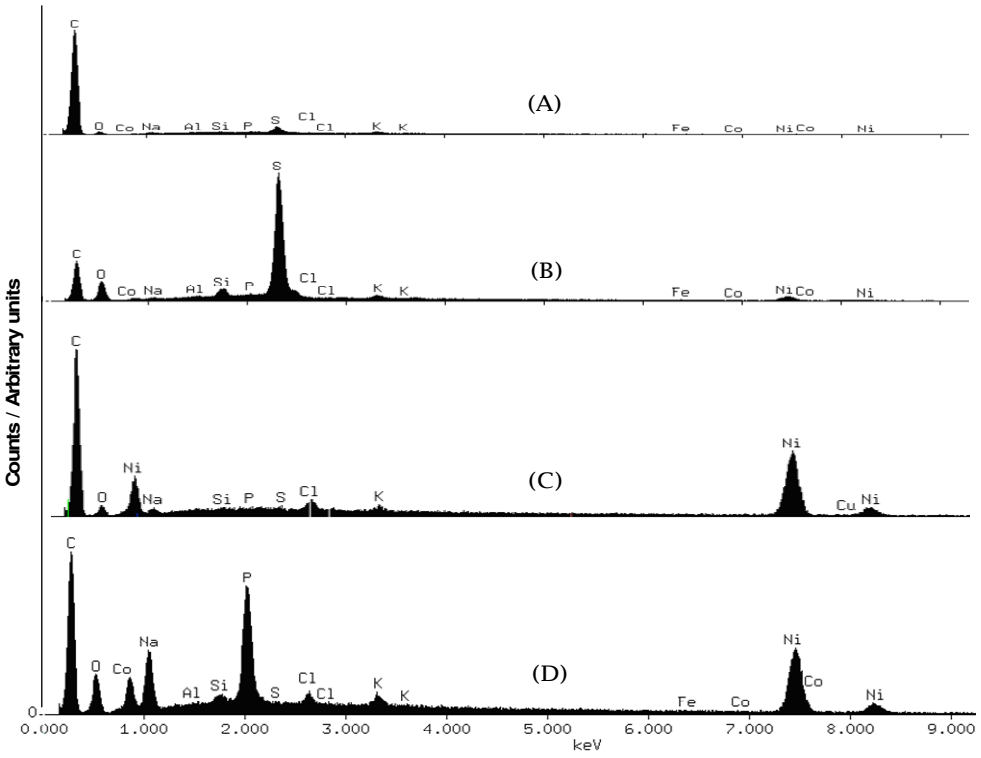

Figure 3.2: Typical EDX plots of the (a) bare EPPGE, (b) EPPGE-SWCNT, (c) EPPGE-SWCNT-Ni, and (d) EPPGE-SWCNT-NiO.

Traces of nickel impurities on the acid-treated and washed SWCNTs indicate these metal impurities are intrinsic to the Aldrich SWCNTs used in this study and cannot be completely removed. A similar result has recently been reported by Jurkschat et al. for HiPCo SWCNTs found to contain iron impurities [3]. The EDX profile of EPPGE-SWCNT-Ni (c) and EPPGE-SWCNT-NiO (d) showed well defined nickel peaks, confirming the successful electrodecoration of the EPPGE-confined SWCNTs. The occurrence of P and Na peaks in the EDX of EPPGE-SWCNT-NiO is ascribed to the treatment of the electrode with sodium phosphate buffer solution while the enhanced oxygen peak confirms the modification of the electrode to its oxide form. Similar trend in the SEM images and EDX profiles were observed for the Fe- and Co-based electrodes (not shown).

3.2 Comparative Redox Chemistry of modified EPPGEs in Aqueous Solution

Figure 3.3 shows examples of the voltammetric responses of the bare and modified EPPGEs (EPPGE-NiO, EPPGE-SWCNT, EPPGE-SWCNT-NiO, EPPGE-SWCNT-FeO and EPPGE-SWCNT-CoO) in 0.1 M phosphate buffered solution (pH 7.0). Successful integration of the metals and metal oxides films with the SWCNTs was observed, confirmed by features such as (i) the presence of the well-defined redox waves of the M(II)/M(III) (M = Ni, Fe and Co; $E_{1/2} \approx 0.45$ V vs Ag|AgCl, sat'd KCl); (ii) the increased current response following the incorporation of the metal particles with the SWCNTs, and (iii) the high background current of the EPPGE-SWCNT-MO compared to other electrodes. These metal oxide nanoparticles exhibit electrochemical stability as the redox peak (II) remained essentially the same even after 50th scan. Some other important features in Figure 3.3 are (i) EPPGE-SWCNT exhibited a pair of weak redox peak ($E_a \approx -0.01$ V and $E_c \approx -0.30$ V), which is typical of immobilized SWCNTs at a carbon electrode. The origins of the broad

cathodic couples (I/I') are the redox processes of the SWCNTs and/or overlapped processes of the M(I)/M(II) and SWCNTs, while the other couple (II/II') are due to the redox processes of the M(II)/M(III). The voltammograms are unsymmetrical with the ratios of the oxidation to reduction charges larger than unity, which are characteristic of quasi-reversible behaviour [4].

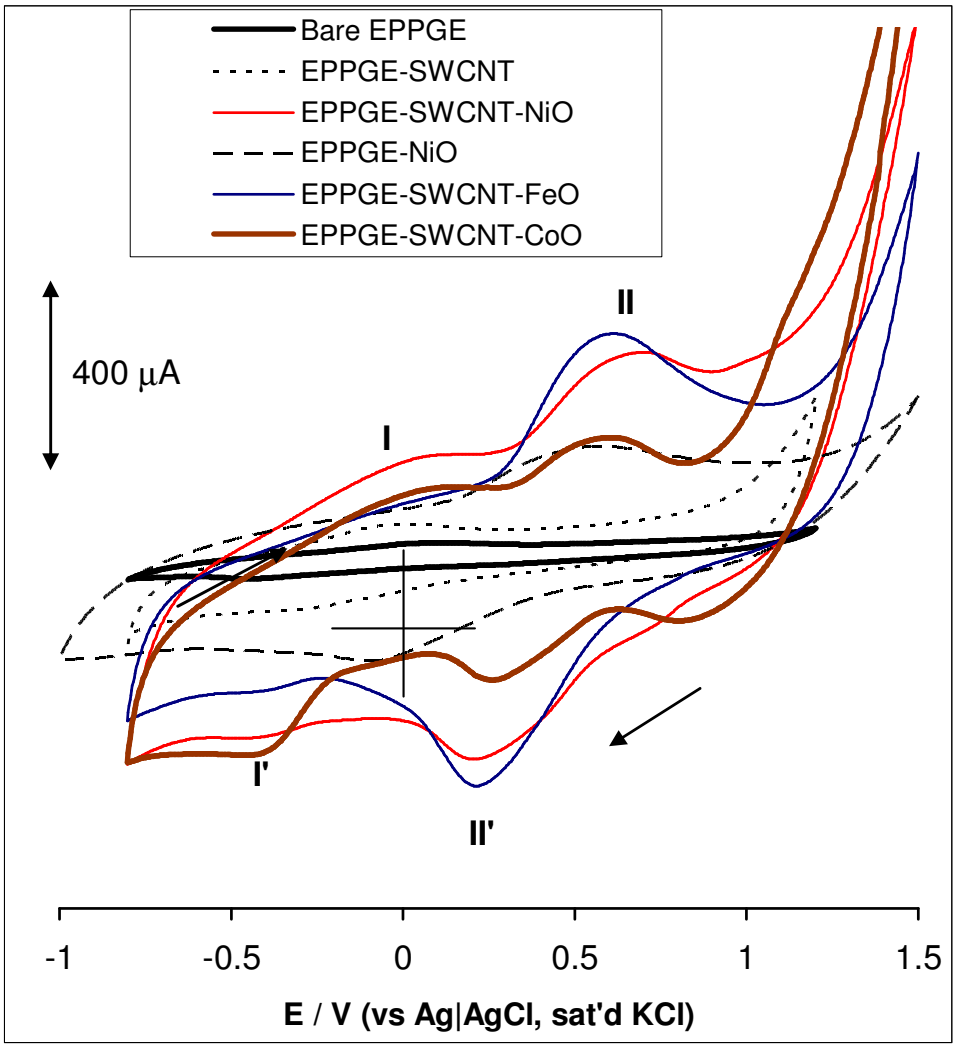

Figure 3.3: Examples of voltammetric evolutions of the bare-EPPGE and modified EPPGEs in 0.1 M pH 7.0 PBS. Scan rate = 50 mV/s. The voltammograms of the modified EPPGEs were obtained after 20 continuous scans. Other scans have been omitted for clarity.

An interesting observation here is the significant decrease in the peak-to-peak separation potential (ΔE) value of the M(II)/M(III)

redox process in the presence of SWCNTs (ΔE = 0.37, 0.42 and 0.50 V for CoO, FeO and NiO, respectively) compared to the absence of SWCNTs (ΔE = 0.70 V). Also, the electrochemical response of the cobalt based electrode is lower than those of the iron and nickel based electrodes. In general, the results suggest the ability of the SWCNTs to serve as efficient conducting carbon materials for electronic communication between the metal nanoparticles and the underlying carbon electrode, EPPGE.

3.3 Comparative electrocatalytic oxidation of hydrazine

Figure 3.4 compares the voltammetric evolutions of the various electrodes in 0.1 M Na_2SO_4 containing 1 mM hydrazine. For a clearer picture of the electro-oxidative responses of the electrodes, the observed voltammograms were subtracted from those generated by their respective electrolytes (as exemplified in Figure 3.4b using the EPPGE-SWCNT-Ni). Peaks (I) (broad at ~ 0.0 V), II ($E_{1/2}$ = 0.35 V) and (III) (E_p = 0.60 V) are due to the redox processes of the SWCNTs, nickel and hydrazine oxidation, respectively. In general, peak current (after background current subtraction) of the hydrazine followed this trend: EPPGE-SWCNT-Ni (~ 44 µA) > EPPGE-SWCNT (~ 37 µA) > EPPGE-SWCNT-Fe (~ 26 µA) > EPPGE-SWCNT-CoO (~23 µA) > EPPGE-SWCNT-NiO (~ 21 µA) > EPPGE-SWCNT-Co (~19 µA) > EPPGE-SWCNT-FeO (~ 18 µA) > EPPGE-FeO (~17 µA) > EPPGE-Fe (~ 16 µA) > EPPGE-Ni (~15 µA) ≈ EPPGE-NiO ≈ Bare EPPGE (~ 15 µA). The oxidation peak of the EPPGE-SWCNT-Ni appeared at about 0.6 V while others occurred at slightly more positive potentials (≥ 0.66 V). The EPPGE modified with metal and metal oxide layers showed weak oxidation peak at more positive potential (*ca.* 0.1 V), suggesting that in the experimental conditions employed in this study, metal and metal oxide layers did not show activity towards hydrazine.

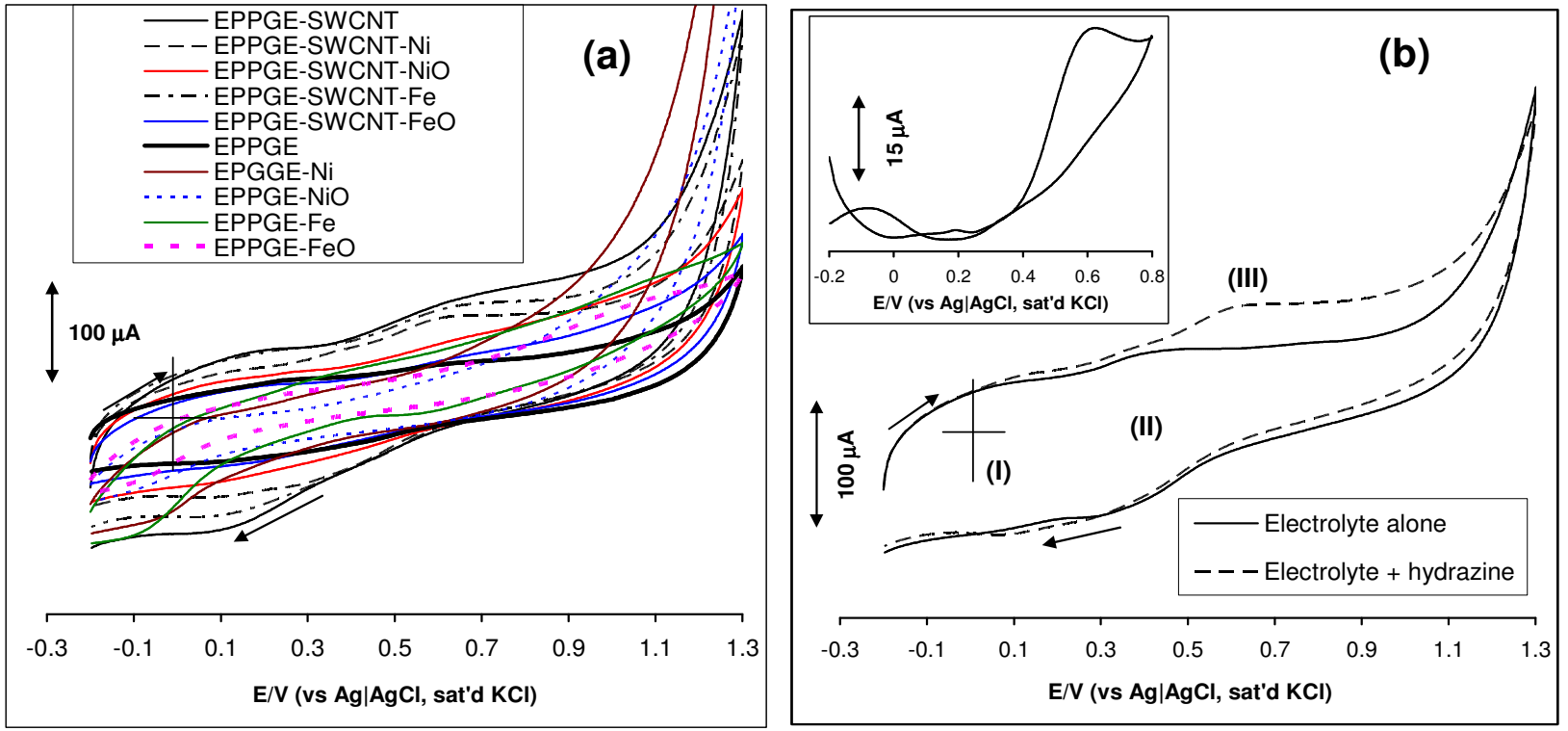

Figure 3.4: (a) Examples of cyclic voltammograms recorded at the various electrodes in 0.1 M Na_2SO_4 solution containing 1 mM hydrazine, and (b) comparative cyclic voltammograms recorded at the EPPGE-SWCNT-Ni in 0.1 M Na_2SO_4 with and without hydrazine. Inset of (b) is the background substracted hydrazine response of the EPPGE-SWCNT-Ni. Scan rate = 25 mVs^{-1}.

The response of the EPPGE-SWCNT is associated with larger background (capacitive) current compared to other electrodes, which is characteristic of acid-treated SWCNTs [5]. The response of SWCNT towards hydrazine oxidation is somewhat controversial. For example, while Guo and Li [6] did not observe any electro-oxidation of hydrazine at SWCNT-paste electrode, Banks and co-workers have consistently observed electro-oxidation of hydrazine at basal plane pyrolytic graphite electrodes modified with either MWCNTs [7,8] or SWCNTs [1,3] which they attributed to the presence of iron oxide impurities. Since the EDX results for the Aldrich SWCNTs (B) did not show iron oxide impurities and no dramatic current responses with both the EPPGE-SWCNT-Fe and EPPGE-SWCNT-FeO was obseved, the influence of iron oxide influencing the electro-oxidation of hydrazine was ruled out; the most likely metal catalyst impurities are the nickel and its oxides. The better electrochemical response exhibited by the EPPGE-SWCNT-Ni compared to other electrodes could be due to the synergistic activities of SWCNTs and Ni particles. The low current response of the metal oxide based electrodes is interesting in that, up to now, for example, only carbon electrodes modified with nickel oxide nanoparticles have been reported for electrocatalytic detection. For example, Salimi *et al.* have used GCEs modified with nickel oxide or cobalt oxide nanoparticles to study the electrochemistry of haemoglobin [9,10], hydrogen peroxide [11], catalase [12] and glucose oxidase [13]. The low response of the nickel oxides modified electrode is attributed to surface layer passivation during electrode modification which results in the layers acting as insulator to charge transfer. Following the better electroactivity of the EPPGE-SWCNT-Ni over the other electrodes, all subsequent studies in this work, unless otherwise stated, were focussed on this electrode.

3.4 Electrochemical impedimetric studies

Insights into the electro-oxidation process of hydrazine at these electrodes were obtained from electrochemical impedance spectroscopy (EIS), at a fixed potential (0.6 V vs Ag/AgCl, sat'd KCl). EIS is a powerful, non-destructive and very informative technique for probing molecules at surfaces. For example, it provides vital information about the charge transfer phenomenon across the electrode|electrolyte interface [14-19]. Figure 3.5 shows examples of the impedance spectra (Nyquist plots) obtained with the electrodes, EPPEGE-SWCNT, EPPGE-SWCNT-Fe, EPPGESWCNT-Ni and EPPGESWCNT-Co at frequencies between 10 kHz and 0.1 Hz.

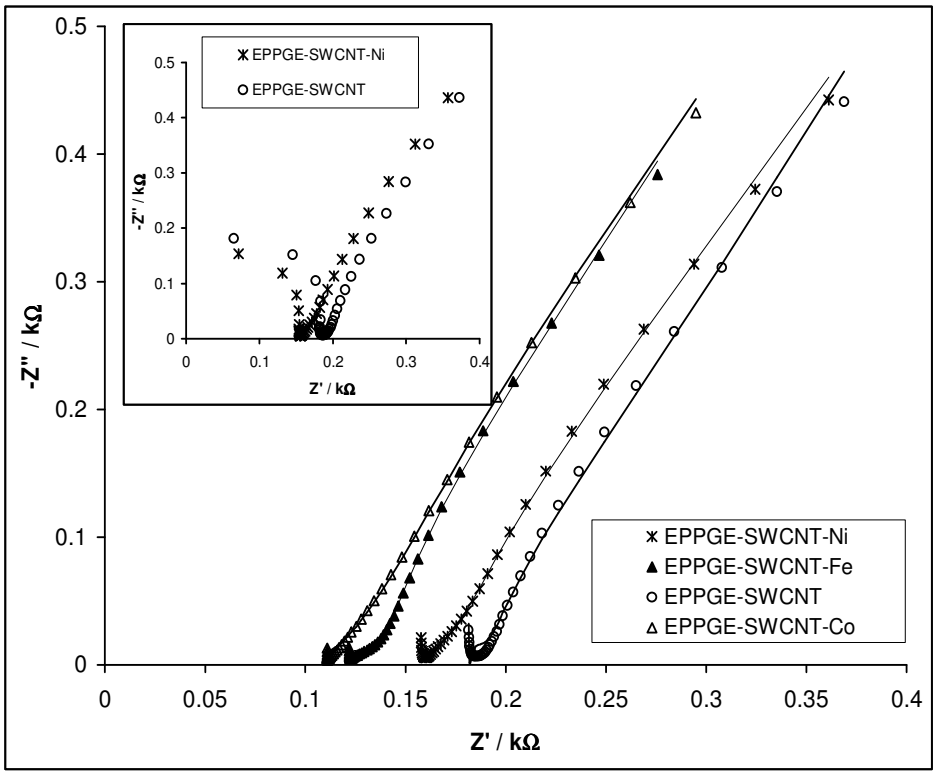

Figure 3.5: Examples of typical Nyquist plots of modified EPPGEs obtained in 0.1 M Na_2SO_4 containing 1 mM hydrazine, between 10 kHz and 0.1 Hz. Inset are similar plots obtained 100 kHz and 0.1 Hz. The data points are experimental while the solid lines represent fitted (theoretical) spectra obtained from the proposed equivalent circuit model shown in figure 5b.

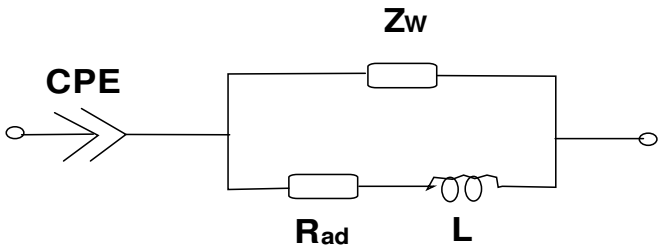

Figure 3.5b: Equivalent circuit model used in fitting the spectra obtained in Figure 3.5a.

The impedance spectra were rather complicated, showing small and distorted semicircle in the high frequency region. Several efforts to obtain a suitable equivalent circuit, including the original Randles model [1] that describes 'true' Faradaic process (i.e., true charge transfer at the electrode|solution interface) were unsuccessful. However, the equivalent circuit model (Figure 3.5b), which incorporates the constant phase element (CPE) and an inductor *L,* yielded satisfactory results as evident from the low percentage error values as evident in Table 3.1. These EIS data were obtained from fitting the equivalent cirquits after several iterations. Presently, the impedance behaviour of the electro-oxidation of hydrazine is virtually non-existent. From the abstract of the only existing report on the electro-oxidation of hydrazine, carried out in alkaline solution on Pd dispersed over graphite cloth, by Duarte *et al*. [20], it is understood that the impedance behavior of the system was also complex. The complexity of the spectra was attributed to several factors including electrode structure, interfacial graphite properties and reaction kinetics. The authors [20] also observed small and distorted semicircle in the high frequency region which they attributed to the porous structure of this carbon-based electrode. The complex impedance behaviour observed in this system may also be associated to the same factors as interpreted by Duarte *et al*. [20].

Table 3.1: Impedance data ($E_{1/2}$ = 0.6V) for the electrocatalytic oxidation of 10^{-3} M Hydrazine (between 10 kHz and 0.1 Hz) on the modified and unmodified EPPGE-electrodes. All values were obtained from the fitted impedance spectra after several iterations using the circuits. Note that the values in parentheses are errors of data fitting.

Electrodes	Q / mF	N	Z_w / μΩcm^2	L / mHcm^2	R_{ad} / μΩcm^2
EPPGE	0.32 ±0.02	0.62 ±0.02	1.85 ±0.12	0.75 ±0.08	32.60 ±0.98
EPPGE-SWCNT	0.49 ±0.03	0.84 ±0.02	3.92 ±0.21	0.93±0.09	45.16 ±0.71
EPPGE-SWCNT-Ni	0.47 ±0.03	0.81 ±0.02	3.67 ±0.19	0.64 ±0.06	32.94 ±0.47
EPPGE-SWCNT-Fe	0.53 ±0.02	0.84 ±0.01	5.34 ±0.26	0.54 ±0.04	31.39 ±0.34
EPPGE-SWCNT-Co	0.50±0.02	0.80±0.01	5.85±0.28	0.50±0.04	26.23±0.35
EPPGE-SWCNT-NiO	0.37 ±0.02	0.82 ±0.02	2.42 ±0.16	0.39 ±0.04	24.10 ±0.33
EPPGE-SWCNT-FeO	0.28 ±0.01	0.73 ±0.01	8.62 ±0.45	0.41 ±0.04	22.48 ±0.38
EPPGE-SWCNT-CoO	0.35±0.02	0.84±0.02	3.69±0.22	0.36±0.04	19.95±0.29

The absence of the solution resistance in the equivalent circuit model suggests that at high frequency the spectra (semi-circle) could possibly extend to the zero point of the real and imaginary impedance plots. Figure 3.5 (inset) shows Nyquist plots carried out between 100 kHz and 0.1 Hz, indicating the possibility of obtaining such semi-circle loop extending the zero point. In this electrical equivalent circuit (Figure. 3.5b), R_{ad} (resistance to adsorption) and *L* are well known as electrical elements associated with the adsorption of reaction intermediate(s) [21-23], clearly suggesting the involvement of the hydrazine intermediate products in the overall electrooxidative process. Duarte *et al*. [20] also detected the existence of an adsorbed intermediate in their system. In electrocatalytic reactions, it is known that inductive behaviour takes place when the Faradaic current is governed by the occupation of an intermediate state [21,23]. The R_{ad} value is therefore interpreted here as the consequence of the adsorption of the intermediate(s) on the electrodes. The R_{ad} values of the metal oxide films are slightly less than those of their metal films, suggesting that the adsorption process is less pronounced at the metal oxides films. *CPE* is ascribed to the geometrical or energetic inhomogeneity of the surface and it is related to *n*. The *n* is a factor describing the deviation from the ideal capacitive behaviour (i.e., n = 1.0). Thus, the *n* value of less than the ideal 1.0 is indicative of pseudocapacitaive processes confirming the presence of the CPE in the circuit. The Warburg (Z_w) impedance relates to the semi-infinite linear diffusion. This occurrence of the inductance was attributed to to the electrode, possibly due to the intermediate absorbed species during the electro-oxidative reactions of hydrazine (further discussed below).

More information on the electrical properties of the electrodes during hydrazine oxidation is provided by closer look at the Bode plot (Figure 3.6).

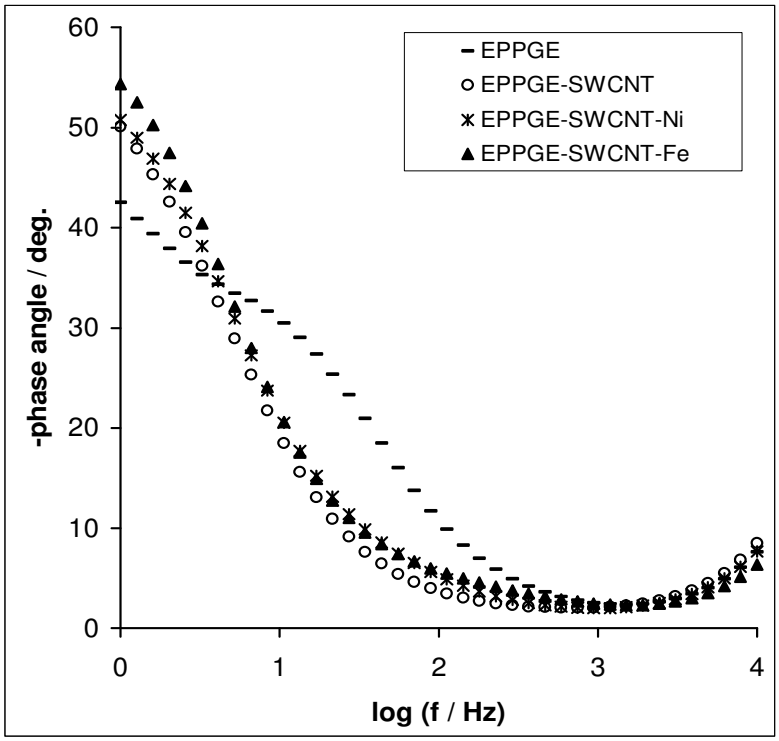

Figure 3.6: Examples of typical Bode plots of modified EPPGEs obtained in 0.1 M Na_2SO_4 containing 1 mM hydrazine, between 10 kHz and 0.1 Hz.

The appearance of a dip or curve in the high frequency region (Figure 3.6) rather than a peak, normally observed for solution resistance (R_s) in the high frequency region, could indicate the dominance of the inductance phenomenon over the solution resistance. The peak at about -35^o depicts the relaxation process of the EPPGE|solution interface; the disappearance of this peak confirms the modification of the EPPGE and replacement by the EPPGE-SWCNT-M Film|solution interface.

Inductive behaviour at high frequency range is thought to be due to either the (i) instrumental artifacts, or (ii) the inductance of the electrode, or (iii) the inductance of the connecting wires [24]. To attempt to rule out (i) and (iii), the experiment was repeated for ten times, but same results were obtained. To provide some insights into the possibility of the electrode itself, i.e., possibility (iii), it was thought to be necessary to carry out the experiment in a

simple redox system. The cyclic voltammetric and impedance spectral evolutions of the EPPGE-SWCNT and EPPGE-SWCNT-Ni in the presence of simple redox probe, $[Fe(CN)_6]^{4-}/[Fe(CN)_6]^{3-}$) were examined. As shown in Figure 3.7, the voltammograms showed redox peak at range -0.20 to 0.30 V for the EPPGE-SWCNT and broad redox peak at 0.45 V for the EPPGE-SWCNT-Ni. The broad peak of the EPPGE-SWCNT-Ni was attributed to possible overlap of the $[Fe(CN)_6]^{4-}/[Fe(CN)_6]^{3-}$ and Ni(II)/Ni(III) redox processes.

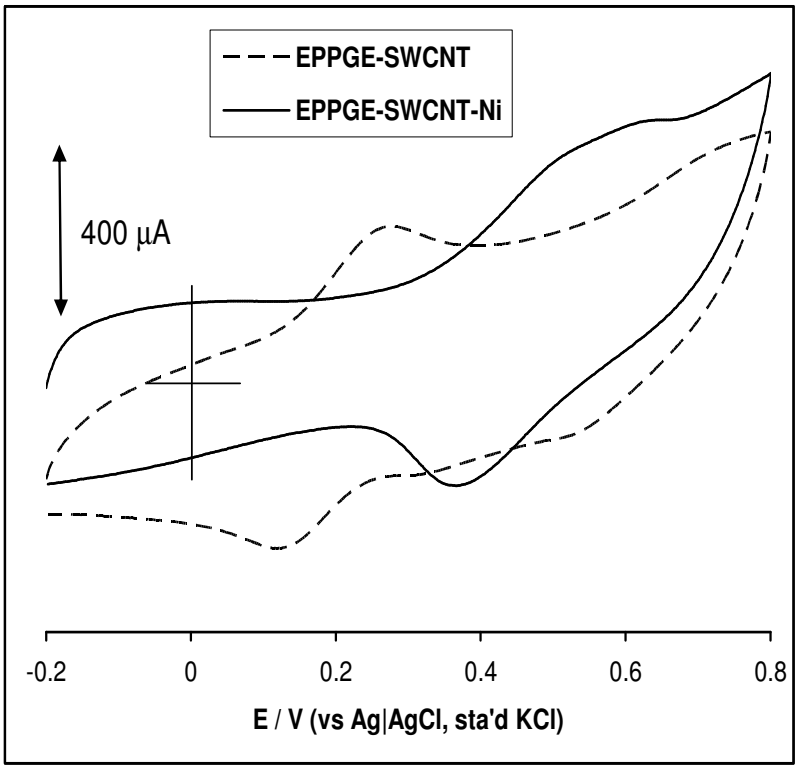

Figure 3.7: Typical comparative cyclic voltammetric evolutions of the electrodes (EPPGE-SWCNT and EPPGE-SWCNT-Ni) in 5 mM $[Fe(CN)_6]^{4-}$ / $[Fe(CN)_6]^{3-}$ solution (PBS pH 7.0). Scan rate = CVs (50mV/s).

Thus, the EIS was perfomed at 0.3 V for both electrodes and also at 0.45 V for the EPPGE-SWCNT-Ni. The Nyquist plots in Figure 3.8 show the experimental data fitted with the equivalent model (Figure 3.8b).

It should be clearly seen that, unlike in hydrazine solution, the equivalent circuit model (Figure 3.8b) incorporates the R_s (the solution/electrolyte resistance) with no inductive behaviour. The excellent fitting of the theoretical model (Figure 3.8b) with the experimental spectra clearly justifies the choice of this circuit model. Interestingly, it was noticed from literature [25] that this equivalent circuit exhibits good resemblance to the equivalent circuit of the so-called "electrolyte-insulator-semiconductor (EIS)" sensors. An electrolyte-insulator-semiconductor device comprises a doped semiconductor acting as substrate for a thin insulating layer, normally an oxide or nitride, which can be immersed in an electrolyte containing a fixed concentration of anionic species to be measured. Indeed, the most important message here is the distinct difference between the EIS data in hydrazine solution and data from solution of simple redox probe, which clearly indicate that these results are not just the consequences of electrode geometry, but electrode mechanisms (notably adsorption phenomena). More detailed study is being undertaken for the EIS evolutions for these electrodes.

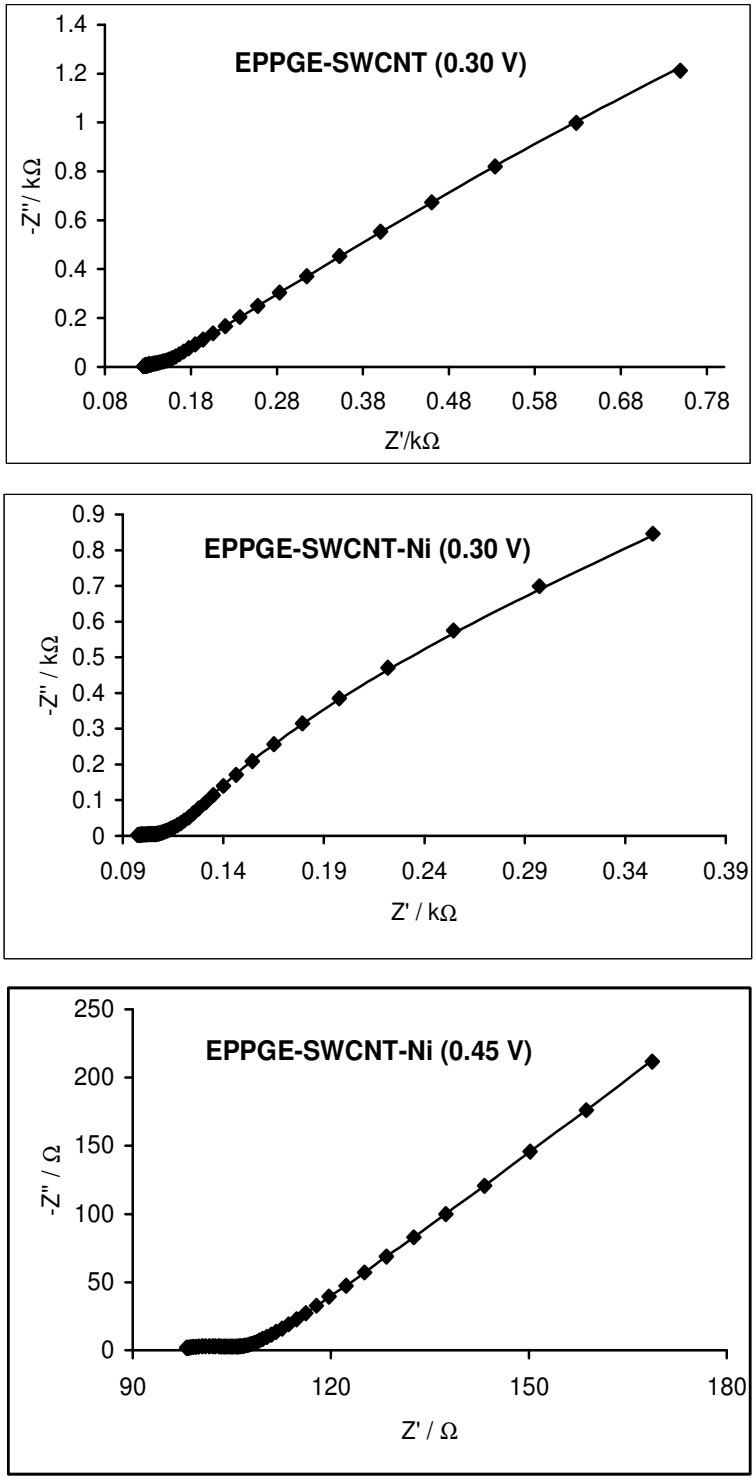

Figure 3.8a: Typical Nyquist plots of the of the electrodes obtained in 5 mM $[Fe(CN)_6]^{4-}$ /$[Fe(CN)_6]^{3-}$ solution (PBS pH 7.0) at fixed potential of 0.30 V and 0.45 V vs Ag|AgCl sat'd KCl.

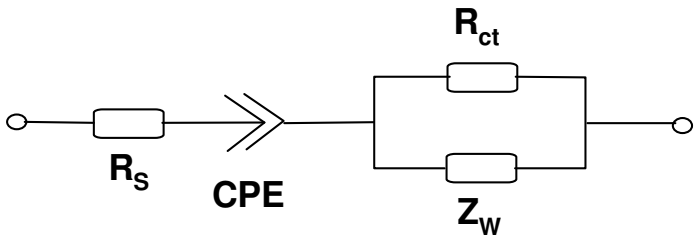

Figure 3.8b: Equivalent circuit model used in fitting the spectra obtained in Figure 3.8a.

3.5 Effect of varying scan rates

Cyclic voltammetric experiments were carried out with a view to establishing the impact of scan rates (ν) at constant concentration (0.01 M) of the hydrazine in 0.1 M Na_2SO_4 solution (Figure 3.9). It was observed that hydrazine peak at 0.6 V and the Ni(II)/Ni(III) redox peak at 0.2 V simultaneously increase with increase in scan rates (scan rates ranging from 10 – 200 mVs^{-1}). At > 100 mVs^{-1} (see inset of Figure 3.6) the Ni(II)/Ni(III) redox process became more pronounced than the hydrazine peak. Their is no firm explanation for this surprising and rare occurrence at this moment, but it may not be unconnected with electrode fouling by intermediate products (radicals) of the hydrazine electro-oxidation (due to adsorption) coupled with the efficient reductive activity of hydrazine solution towards nickel ions as reported by the Bettahar group [26,27]. The plot of peak current versus square root of scan rate ($\nu^{1/2}$) was linear (R^2 = 0.9938), an indication of diffusion-controlled electro-oxidative process. The current function plot (Figure 3.9b) confirms coupled chemical reaction (EC_{cat}) for hydrazine. Recall that the electrooxidation of hydrazine in carbon-based electrodes follows a four-electron process generating nitrogen and water as products.

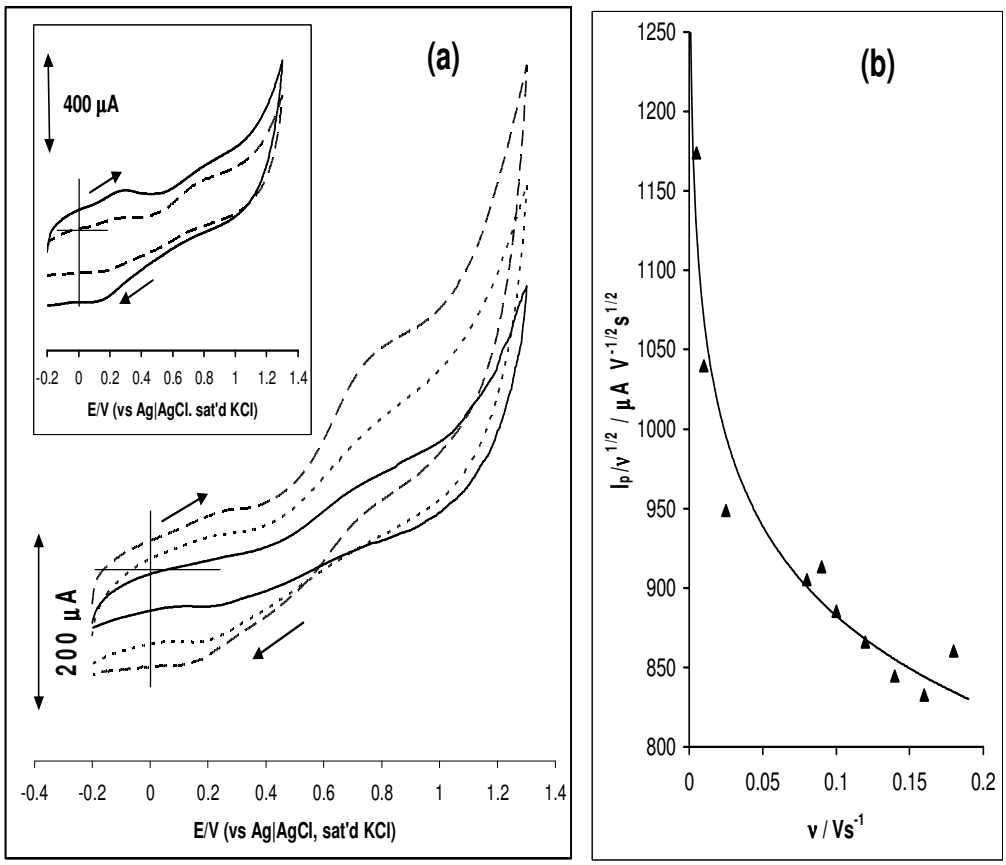

Figure 3.9: (a) Examples of cyclc voltammetric evolutions of EPPGE-SWCNT-Ni obtained in 0.1 M Na_2SO_4 containing 1 mM hydrazine at scan rates 10, 25 and 50 mVs^{-1}(inner to outer). Inset compares voltammograms obtained at 50 and 140 mVs^{-1} (inner to outer). (b) Current function plot, $I_p/\nu^{1/2}$ vs ν.

Lin and Bocarsly [28] had elegantly described the electrooxidation of hydrazine at nickel ferricyanide modified electrode, proposing series of very fast sequential charge transfer processes with intermediates that also adsorb on the electrode. From the results above, it might thus be concluded here that the electrooxidation process of hydrazine on the electrode system does not only occur at the SWCNT-metal film|solution interface, due to its small size [28], hydrazine molecule has the possibility of penetrating the SWCNT-metal film. Three main rate-limiting possibilities could be (i) mass transport of hydrazine in the solution, (ii) diffusion or permeation of the hydrazine and/or its intermediates

through the SWCNT-Metal film, and (iii) charge transport through the film (or rate at which the metal catalyst is regenerated). On the basis of the information, the following general mechanism for the oxidation of hydrazine can be suggested. The redox process of the SWCNT-confined metal (M = Ni or Fe or Co) species is:

$$(M^{3+})film \rightleftharpoons (M^{2+})film + e- \quad (3.1)$$

The interaction of the M^{3+} with aqueous hydrazine results to the regeneration of the M^{2+} and the formation of hydrazine oxidation intermediates:

$$(M^{3+})film\,(Hydrazine) \longrightarrow (M^{2+})film + Intermediates + e- \quad (3.3)$$

The oxidation intermediate(s) are further oxidized to the final product(s), via similar mediated electro-oxidation process:

$$(M^{3+}) + Hydrazine\ (aq) \longrightarrow (M^{3+})film\,(Hydrazine) \quad (3.2)$$

$$(M^{3+})film\ (Intermediates) \longrightarrow (M^{2+})film + Products \quad (3.4)$$

The enhanced current response of the Ni^{2+}/Ni^{3+} redox process at high scan rates suggest in Figure 3.6 (inset) may be ascribed to this efficient regeneration of the Ni^{2+} ions on the SWCNTs surface by hydrazine and its oxidation products.

3.6 Chronoamperometric investigations

Further studies on electro-oxidative processes of hydrazine solution at the EPPGE-SWCNT-Ni were investigated using chronoamperometric experiments. Figure 3.10 shows typical results obtained from chronomperometric experiments performed by polarizing the working electrode potentials at 0.60 V. A linear relationship between background-subtracted transient current and hydrazine concentrations was obtained as:

$$I/\mu A = (0.52 \pm 0.02)\,[hydrazine]/\mu M - (9.92 \pm 0.85) \quad (3.5)$$

The sensitivity was calculated as 0.52 ± 0.02 AM^{-1} (R^2=0.9954) while the limit of detection (LoD = 3.3 s/m [29], where *s* is the relative standard deviation of the intercept and *m* the slope of the linear current versus the concentration of hydrazine) was 5.3 ± 0.1 µM. Table 3.2 compares the linear concentration range, LoD and sensitivity value obtained in this study with literature values [30-37].

The catalytic rate constants (k) for the oxidation of hydrazine at both EPPGE-SWCNT-Ni and EPPGE-SWCNT-Fe were estimated from the relationship [38,39] (Equation 3.6):

$$\frac{I_{cat}}{I_{buff}} = \pi^{1/2}(kCt)^{1/2} \qquad (3.6)$$

where I_{cat}, I_{buff}, *k* and t are already defined (Chapter 1, section 1.3). From the plots of I_{cat}/I_{buff} vs $t^{1/2}$ at different hydrazine concentrations (not shown), and a plot of the slopes vs square root of the hydrazine concentrations (exemplified with EPPGE-SWCNT-Ni in Figure 3.8 inset), *k* values were approximately the same, (2.2 ± 0.18) x 10^4, (2.0 ± 0.16) x 10^4 and (0.24 ± 0.02) x 10^4 cm^3 $mol^{-1}s^{-1}$ for EPPGE-SWCNT-Ni, EPPGE-SWCNT-Fe and EPPGE-SWCNT-Co respectively, suggesting that the electrocatalytic oxidation of hydrazine was least favoured at the EPPGE-SWCNT-Co but essentially the same for both EPPGE-SWCNT-Ni and EPPGE-SWCNT-Fe.

The diffusion coefficient, *D*, of hydrazine at the EPPGE-SWCNT-Ni was estimated from the Cottrell Equation [40]:

$$I = \frac{nFAD^{1/2}C}{\pi^{1/2}t^{1/2}} \qquad (3.7)$$

where all symbols are already defined (Chapter 1, section 1.3) and included on the list of symbols. Assuming n ≈ 4 [26-28]. From the experimental plots of I versus $t^{-1/2}$ at different concentrations (not shown), the diffusion coefficient D of hydrazine was calculated as (2.5 ± 0.24) x10^{-5} cm^2s^{-1}.

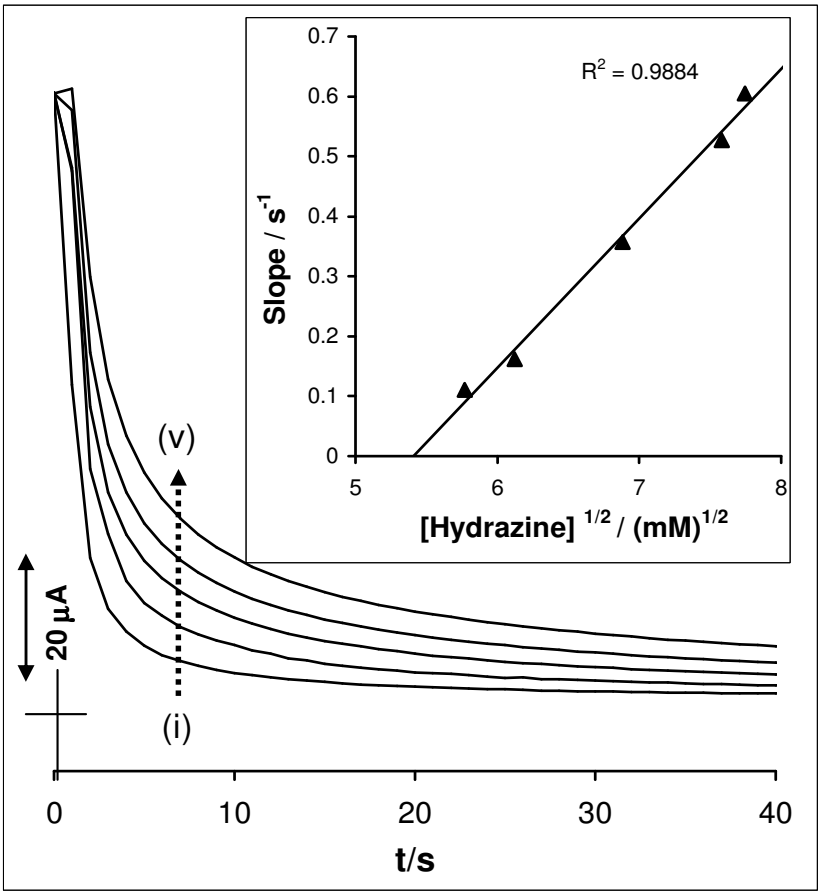

Figure 3.10: Chronoamperometric evolutions of the EPPGE-SWCNT-Ni in 0.1 M Na_2SO_4 solution containing different concentrations of hydrazines (0.0, 33.3, 47.4, 50.5 and 54.5 µM (from (i) to (v)) at fixed potential of 0.6V. Inset is plot of slope vs square root of the concentration of hydrazine.

Table 3.2: Comparative analytical data for the detection of hydrazine at chemically modified electrodes

Electrodes	**Methods**	**Analytical Parameters**			
		LCR / μM	**LoD/ μM**	***Sensitivity*** **/μAμM^{-1}**	**Ref**
CM-MWCNT-GCE	CA	2.0 – 44	1.4	0.0229	30
CCE-NiHCF	CV	20 - 2000	8.0		31
IMWCNTCPE	DPV	0.6-8.0 8.0-100.0	0.29	0.167 0.014	32
MnHCF-graphite wax	CA	33.3– 8,180,000	6.65	0.0475	33
TCNQ-CPE	CA	2.0–100.0	0.6	0.36	34
MnTPPS-GCE	CA	0.25–250	0.03	-	35
Rutheniumcomplex-GCE	CA	10.0-90.0	8.5	-	36
ST-NiTsPc	CA	100-600	10	–	37
EPPGE-SWCNT-Ni	CA	33.3-54.5	5.3 ± 0.1	0.52 ± 0.02	This work

CA: Chronoamperometry; CV: Cyclic voltammetry; DPV: Differential pulse voltammetry; CM-MWCNT-GCE:Curcumin- multi-walled carbon nanotube modified glassy carbon electrode; CCE-NiHCF: carbon ceramic electrode (CCE) modified with nickel hexacyanoferrate; IMWCNTCCE: indenedione derivatives multi-walled carbon nanotube modified carbon ceramic electrode; MnHCF:Manganese hexacyanoferrate graphite wax modified electrode; TCNQ-CPE: Tetracyanoquinodimethanide-titanium oxide modified carbon paste electrode; MnTPPS-GCE: *meso*-tetra(4-sulphonatephenyl)porphyrinate manganese(III) complex glassy carbon modified electrode; Glassy carbon electrodes modified with (5-amino-1,10-phenanthroline)bis(bipyridine)ruthium(II) chloride hydrate, [(bpy)(2)Ru(5-phenNH(2))]Cl(2).H(2)O; ST-NiTsPc: Nickel tetrasulfonated phthalocyanine (NiTsPc) immobilized onto titanized silica gel.

It has been shown that edge plane pyrolytic graphite electrodes modified with Aldrich SWCNTs electro-decorated with nickel and iron nanoparticles exhibit comparable electrochemical response in buffered aqueous solution (pH 7.0) and towards electro-

oxidation of hydrazine in Na_2SO_4 solution. Also, it was established from electrochemical impedance spectroscopy that these SWCNT-metal hybrids are rather complicated and follow electrical equivalent circuit model typical of adsorption-controlled charge transfer kinetics. EIS data obtained in a simple redox probe, ($[Fe(CN)_6]^{3-}$/($[Fe(CN)_6]^{4-}$), showed that EPPGE-SWCNT and EPPGE-SWCNT-Ni followed electrical equivalent circuit models typical of partial charge transfer or adsorption-controlled kinetics with some resemblance to the behaviour of electrolyte-insulator-semiconductor sensors. These differences in the data clearly, and for the first time, provide some insights into the electrooxidative mechanism of hydrazine at carbon electrodes modified with single-walled carbon nanotubes decorated with metal and metal oxide films.

References

1. J. Kruusma, N. Mould, K. Jurkschat, A. Crossley, C.E. Banks, *Electrochem. Commun.* 9 (2007) 2330.

2. M. Pumera, *Langmuir* 23 (2007) 6453.

3. K. Jurkschat, X. Ji, A. Crossley, R.G. Compton, C.E. Banks, *Analyst* 132 (2007) 21.

4. A.J. Bard, L.R. Faulkner, *Electrochemical Methods: Fundamentals and Applications*, 2nd ed, John Wiley & Sons, Hoboken NJ (2001).

5. C. Peng, J. Jin, G.Z. Chen, *Electrochim. Acta* 53 (2007) 525.

6. D-J. Guo, H-L. Li, *J. Colloid Interf. Sci.*, 286 (2005) 274.

7. C.E. Banks, A. Crossley, C. Salter, S.J. Wilkins, R.G. Compton, *Angew. Chem. Int. Ed.* 45 (2006) 2533.

8. C.P. Jones, K. Jurkschat, A. Crossley, R.G. Compton, B.L. Riehl, C.E. Banks, *Langmuir* 23 (2007) 9501.

9. A. Salimi, R. Hallaj, S. Soltanian, *Biophys. Chem.* 130 (2007) 122.

10. A. Salimi, E. Sharifi, A. Noorbakhsh, S. Soltanian, *Electrochem. Commun.* 8 (2006) 1499.
11. A. Salimi, R. Hallaj, S. Soltanian, H. Mamkhezri, *Anal. Chim. Acta* 594 (2007) 24.

12. A. Salimi, E. Sharifi, A. Noorbakhsh, S. Soltanian, *Biophys. Chem.* 125 (2007) 540.

13. A. Salimi, E. Sharifi, A. Noorbakhsh, S. Soltanian, *Biosens. Bioelectron.* 22 (2007) 3146.

14. E. Barsoukov, J.R. Macdonald (eds.), *Impedance Spectroscopy: Theory, Experiment, and Applications*, 2nd ed. Hoboken NJ Wiley (2005).

15. X. Wu, H. Ma, S. Chen, Z. Xu, A. Sui, *J. Electrochem. Soc.* 146 (1999) 1847.

16. G. Nurk, H. Kasuk, K. Lust, A. Janes, E. Lust, *J. Electroanal. Chem.* 553 (2003) 1.

17. C. Hu, X. Dang, S. Hu, *J. Electroanal. Chem.* 572 (2004) 161.

18. T. Thomberg, J. Nerut, E. Lust, *J. Electroanal. Chem.* 586 (2006) 237.

19. P.M.S. Monk, *Fundamentals of Electroanalytical Chemistry*, John Wiley and Sons, Chichester, 2001, p.172.

20. M.M.E. Duarte, M.M. Stefenel, C.E. Mayer, *J. Arg. Chem. Soc.* 90 (2002) 111.

21. J. Bisquert, H. Randriamahazaka, G. Garcia-Belmonte, *Electrochim. Acta* 51 (2005) 627.

22. M. Jafarian, M.G. Mahjani, H. Heli, F. Gobal, H. Khajehsharifi, M.H. Hamedi, *Electrochim. Acta* 48 (2003) 3423.

23. S. Majdi, A. Jabbari, H. Heli, A.A. Moosavi-Movahedi, *Electrochim. Acta* 52 (2007) 4622.

24. Research Solutions & Resources available online at: http://www.consultrsr.com/resources/eis/induct2.htm (accessed 24 February 2008).

25. E. Bonanos, B.C.H. Steele, E.P. Butler, in: *Impedance Spectroscopy: TheoryExperiment, and Applications*, 2nd ed, E. Barsoukov and J.R. Macdonald eds.), Wiley, Hoboken, New Jersey, 2005, Chap. 4, p 284.

26. A-G. Boudjahem, S. Monteverdi, M. Mercy, M.M. Bettahar *Langmuir* 20 (2004) 208.

27. R. Wojcieszak, M. Zielinski, S. Monteverdi, M.M. Bettahar *J. Colloid Interf. Sci.* 299 (2006) 238.

28. C. Lin, A.B. Bocarsly, *J. Electroanal. Chem. Interf. Electrochem.* 300 (1991) 325.

29. G.D. Christian (2004) Analytical Chemistry, 6th ed. John Wiley and Sons New York, p 113.

30. L. Zheng, J.-f. Song, *Sens. Actuat. B* 135 (2009) 650.

31. A. Abbaspour, A. Khajehzadeh, A. Ghaffarinejad, *J. Electroanal. Chem.* 631 (2009) 52.

32. H.R. Zare, N. Nasirizadeh, F. Chatraei, S. Makarem, *Electrochim. Acta* 54 (2009) 2828.

33. D. Jayasri, S.S. Narayanan, *J. Hazard. Mater.* 144 (2007) 348.

34. J.C. Duarte, R.C.S. Luz, F.S. Damos, A.B. Oliveira, L.T. Kubota, *J. Solid State Electrochem.* 11 (2007) 631.

35. M.S.M. Quintino, K. Araki, H.E. Toma, L. Angnes, *Talanta* 74 (2008) 730.

36. J.S. Pinter, K.L. Brown, P.A. DeYoung, G.F. Peaslee, *Talanta* 71 (2007) 1219.

37. E.F. Perez, G.-O. Neto, A.A. Tanaka, L.T. Kubota, *Electroanalysis* 10 (1998) 111.

38. M.H. Pournaghi-Azar, R. Sabzi, *J. Electroanal. Chem.* 543 (2003) 115.

39. K.M. Manesh, P. Santosh, A.I. Gopalan, K-P. Lee, *Electroanalysis* 18 (2006) 894.

40. D. Giovanelli, N.S. Lawrence, S.J. Wilkins, L. Jiang, T.G.J. Jones, R.G. Compton, *Talanta* 61 (2003) 211.